2021

Relationship Between Atmospheric Teleconnections And The Northern Hemisphere'S Circumpolar Vortex

N Bushra
nbushr1@lsu.edu

R V. Rohli

Recommended Citation

Bushra, N., & Rohli, R. V. (2021). Relationship Between Atmospheric Teleconnections And The Northern Hemisphere'S Circumpolar Vortex. *Earth And Space Science, 8* (9) https://doi.org/10.1029/2021EA001802

AGU ADVANCING EARTH AND SPACE SCIENCE

Earth and Space Science

RESEARCH ARTICLE
10.1029/2021EA001802

Relationship Between Atmospheric Teleconnections and the Northern Hemisphere's Circumpolar Vortex

Nazla Bushra[1] **and Robert V. Rohli**[1]

[1]Department of Oceanography & Coastal Sciences, College of the Coast & Environment, Louisiana State University, Baton Rouge, LA, USA

Key Points:

- Daily variability of the Northern Hemisphere's circumpolar vortex (NHCPV) is linked to variability in air-sea teleconnection patterns
- NHCPV is more strongly correlated with the extratropical Arctic Oscillation, North Atlantic Oscillation, and Pacific-North American teleconnections than it is correlated to the tropical El Niño/Southern Oscillation
- Linkage between the NHCPV and teleconnection variability is important as the low- and high-frequency variability influences weather systems

Correspondence to:

N. Bushra,
nbushr1@lsu.edu

Citation:

Bushra, N., & Rohli, R. V. (2021). Relationship between atmospheric teleconnections and the Northern Hemisphere's circumpolar vortex. *Earth and Space Science*, *8*, e2021EA001802. https://doi.org/10.1029/2021EA001802

Received 10 APR 2021
Accepted 13 AUG 2021

Author Contributions:

Conceptualization: Nazla Bushra, Robert V. Rohli
Data curation: Nazla Bushra
Formal analysis: Nazla Bushra
Funding acquisition: Robert V. Rohli
Investigation: Nazla Bushra, Robert V. Rohli
Methodology: Nazla Bushra, Robert V. Rohli
Project Administration: Robert V. Rohli
Supervision: Robert V. Rohli
Validation: Nazla Bushra
Visualization: Nazla Bushra

Abstract

The Northern Hemispheric circumpolar vortex (NHCPV) is the hemispheric-scale, middle- and upper-tropospheric wind belt circumnavigating the North Pole. It is delineated by the well-known polar front jet stream, and it bends poleward at ridges and equatorward at troughs at various amplitudes and positions over time. Previous work assessed the accuracy of representing the NHCPV using a new technique through correlations to air-sea teleconnections known to be related to broad-scale, extratropical steering circulation at the monthly scale. Results of that work suggested that the method allows for notable improvements in the calculation of area and circularity of the 500-hPa manifestation of the NHCPV. Because using monthly averaged data to represent the NHCPV may oversimplify analyses, especially for identifying meteorological impacts, this research employs the same technique for identifying the daily NHCPV. Results suggest that CPV area and circularity are even more closely related to variability in the North Atlantic Oscillation (NAO), Pacific/North American pattern, and (especially) Arctic Oscillation (AO) teleconnections, and the El Niño/Southern Oscillation phenomenon at the daily scale than at the monthly scale. A principal components analysis reveals the extent of the interrelationships between the teleconnections and NHCPV area and circularity. Results generally affirm that both the individual teleconnections, especially the NAO and AO, and interdependencies among these teleconnections and others, are strongly related to the NHCPV area and circularity. These findings are important because low- and high-frequency variability in the amplitudes and positions of the undulations in the broad-scale flow influence weather systems that exert important impacts on society.

Plain Language Summary

The broad-scale, west-to-east, upper-level atmospheric flow separates the frigid polar air from the much more moderate temperate air over the middle latitudes. Popularly known as the "polar vortex," this circumpolar vortex (CPV) expands equatorward and contracts poleward, and becomes quasi-circular at times and wavier (with south-to-north or north-to-south components of flow) at other times on its general west-to-east trek around the North Pole. Previous work has defined the CPV's position at a given time using a predetermined, one-size-fits-all elevation at which 500 hPa of atmospheric pressure occurs. Our approach introduced in a previous study is based on the steepest gradient of that elevation. In this study, we demonstrate the effectiveness of this new delineation by showing that the CPV's area and waviness are linked at the daily scale to several known atmospheric circulation features that have been shown previously to be associated with the CPV. Two atmospheric flow patterns—the so-called Arctic Oscillation and the related North Atlantic Oscillation—are particularly closely linked to the Northern Hemisphere's CPV (NHCPV), and the El Niño/Southern Oscillation phenomenon is associated less directly with NHCPV variability. Results will help atmospheric scientists as they use model output of the CPV's position to identify steering patterns that affect daily weather.

1. Introduction

The circumpolar vortex (CPV) is the continuous zone of rapid winds generally flowing cyclonically aloft in the middle-to-upper troposphere circumnavigating each pole. The leading edge of the CPV is the polar front, which steers, supports, and suppresses extratropical surface weather systems by providing upper-level support (or lack thereof) for surface storms. Therefore, knowledge regarding the spatial and temporal variability associated with the CPV can enhance understanding of surface weather and its related impacts.

Bushra and Rohli (2019) identified a new method for identifying the CPV, with diagnostic measurements of the CPV's area, hemispheric zonality in the form of a circularity ratio (R_c—the ratio of the area enclosed

Writing – original draft: Nazla Bushra
Writing – review & editing: Robert V. Rohli

within the Northern Hemisphere's circumpolar vortex [NHCPV] polygon to the area of a circle with a circumference equal to the distance enclosed by the polygon, such that near-zero values represent more amplified ridges/troughs and values near 1.0 represent a more circular NHCPV—Rohli et al., 2005), and centroid location. The daily values from Bushra and Rohli (2019) were aggregated and reported at the monthly scale for direct comparison to Wrona and Rohli's (2007) monthly mean Northern Hemispheric CPV (NHCPV) area and R_c for the months included in Wrona and Rohli's (2007) analysis (April, July, October, December, January, and February). Wrona and Rohli (2007) had used the more conventional approach of defining the NHCPV using a pre-determined 500-hPa isohypse recommended by Frauenfeld and Davis (2003), over the 1979–2001 period. Results from Bushra and Rohli (2019) revealed that although the previous work had represented substantial steps forward, the new technique, which delineates the CPV at the steepest 500-hPa geopotential height gradient along each meridian of longitude, is advantageous because it reveals NHCPV variability that is linked more strongly than the previous techniques to known modulators of monthly circulation variability in the form of atmospheric teleconnections. This result is potentially very important, because, if this result is confirmed at the daily scale, then the available daily indices for the major atmospheric teleconnection patterns could lead to an improved understanding of sub-monthly-scale atmospheric variability, such as floods and severe weather events.

As the new measurement technique has been validated, the purpose of this research is to address the question of how the area and circularity of the NHCPV are linked to teleconnection variability *on a daily scale*. This question is important to address for two reasons: (a) two extreme anomalies of opposite sign within a month could provide the mistaken impression that a teleconnection was in its "average" mode simply because its index near zero; and (b) the main modes of variability in broad-scale atmospheric flow in the form of atmospheric teleconnections are increasingly predictable at long lead times, yet their most important impacts are at the daily time scale in the form of extreme weather events. In addition to the investigation of high-frequency (i.e., daily) variability of the teleconnection patterns taken individually, the association between some teleconnections to each other calls for an examination of the collective linkage between modes of variability in broad-scale flow and the NHCPV. Thus, a principal components analysis (PCA) is implemented to reduce the dimensionality (number of variables) of the data set and reveal the listic links between the teleconnections and NHCPV area and R_c.

This research addresses the following research questions: (a) to what extent does variability associated with tropical versus extratropical atmospheric teleconnections align with variability in the NHCPV area and R_c? (b) How does variability in multiple teleconnections, acting together, align with NHCPV area and R_c? While we acknowledge that geophysical impacts of the El Niño/Southern Oscillation (ENSO) phenomenon require weeks to months to materialize, with different lag times at different times of the year, we include ENSO as part of our analysis, for comparison to the representation of higher-frequency forms of variability in the form of mid-latitude teleconnections.

2. Atmospheric Teleconnections That Influence Extratropical Flow

The identification of major modes of broad-scale atmospheric variability has a rich history, including seminal work by Walker and Bliss (1932), Horel and Wallace (1981), Wallace and Gutzler (1981), and Barnston and Livezey (1987). The most important mode of low-frequency atmosphere-ocean variability is ENSO (Philander, 1990). ENSO is an oscillation between surface atmospheric pressure between the western and eastern equatorial Pacific Ocean. During times when the atmospheric sea level pressure (SLP) is anomalously high (low) in the western tropical Pacific, it is simultaneously low (high) in the eastern tropical Pacific, and this phase corresponds to the El Niño or a "warm event" (La Niña or "cold event") phase in the ocean. Torrence and Compo (1998) explained the implications of wavelet analysis in the atmospheric sciences using the example of the El Niño–Southern Oscillation (ENSO) time series from 1871 to 1997. Among the many indices representing the mode of ENSO variability, the Southern Oscillation index (SOI) is one of the most commonly used (e.g., Li et al., 2021; Ropelewski & Jones, 1987), particularly in atmospheric research, since it is based on normalized SLP differences—between Tahiti and Darwin, Australia, with positive (negative) SOI representing La Niña (El Niño). A second index is more popular in oceanographic work (e.g., Clarke & van Gorder, 2001; Hardiman et al., 2019; Menendez et al., 2008; Zhi et al., 2020) because it

relies on sea surface temperature (SST) departures; this so-called Niño3.4 index is aligned such that positive (negative) values indicate El Niño (La Niña).

Much previous work has investigated the relationship between tropical teleconnections, particularly ENSO, and the NHCPV. The tendencies for El Niño to be followed by shrinking of the NHCPV with a three-season lag (Angell, 1992) and within the season (Frauenfeld & Davis, 2000) has been noted, presumably because of the poleward shift in the steepest gradient of oceanic temperatures (Bushra & Rohli, 2019), but the eastern Pacific sector of the NHCPV expands during an El Niño event (Angell, 1992). Over the periods 1959–2001, Rohli et al. (2005) found that neither the SOI nor the Niño3.4 SST index show significant correlation with either January NHCPV area or R_c. Although Angell and Korshover (1977) had found a tendency for the NHCPV to be contracted when the quasi-biennial oscillation (QBO) was in its westerly phase from 1963 to 1975, Angell (2001) found little evidence for a relationship between the NHCPV area and the QBO over the tropical stratosphere.

Not unexpectedly, extratropical teleconnections, which are driven largely by CPV behavior, have also been evaluated for their influences on weather. The North Atlantic Oscillation (NAO; Barnston & Livezey, 1987; Hurrell, 1995; van Loon & Rogers, 1978; Wallace & Gutzler, 1981) modulates the atmospheric circulation that impacts weather conditions in western Europe and the eastern United States (Higgins et al., 2000; Hurrell & Van Loon, 1997; Kapala et al., 1998). Higuchi et al. (1999) employed multiresolution Fourier transform spectral analysis to resolve the temporal structure of the variation of the NAO from 1865 to 1991 in terms of various frequency components. The NAO index has been used to measure the surface temperature and differences in normalized SLP (Wallace & Gutzler, 1981) between two locations: Ponta Delgada, Azores, and Akureyri, Iceland (Lamb & Peppler, 1987), or it can be derived based on empirical orthogonal function analysis of mid-tropospheric geopotential heights (e.g., Deser & Blackmon, 1993). Positive (negative) phases of the NAO correspond with a large (small) standardized SLP difference between the Bermuda-Azores subtropical anticyclone and the Icelandic Low, and strong (weak) westerlies across the North Atlantic (Wallace & Gutzler, 1981). The positive (negative) NAO is associated with positive (negative) temperatures departures in the eastern United States and northwestern Europe and negative- (positive-) temperature anomalies in the Greenland/Labrador area (Wallace & Gutzler, 1981). PCA has been used to identify modes of variability associated with teleconnections including the NAO (e.g., Martinez-Artigas et al., 2021).

The Arctic Oscillation (AO), characterized by oscillation of atmospheric mass between the Arctic and the mid-latitudes, is another dominant mode of Northern Hemispheric-scale atmospheric variability (Thompson & Wallace, 1998, 2000). The AO pattern influences weather and climate of the vast regions of North America, Europe, and East Asia (e.g., Higgins et al., 2002; Kolstad et al., 2010; Park et al., 2011; Tomassini et al., 2012). A positive (negative) AO index indicates negative (positive) geopotential height anomalies over the Arctic and anomalously high (low) geopotential heights in lower latitudes and causes a "warm (cold) phase" particularly over northern Europe (Thompson & Wallace, 1998). Variability associated with the AO tends to occur on a multitude of time scales, including decadal, with the 1960s through the 1980s dominated by the negative AO phase and the 1990s through the most of the first two decades of the new century dominated by positive AO conditions, with strongly fluctuating signals in recent years.

Several studies (e.g., Ambaum et al., 2001; Rogers & McHugh, 2002; Wanner et al., 2001) have shown that the AO resembles the NAO and there is a strong correlation between them, although their signs and impacts can differ (D. Wang et al., 2005). The frequency-time appearance of NAO is physically more robust, consistent, and relevant to North Atlantic winter climate variability than the AO (Ambaum et al., 2001). The AO and NAO indices are negatively correlated with the area of the NHCPV in winter (represented by December through February) and spring (represented by April; Wrona & Rohli, 2007), such that the positive or "warm" phase is linked to shrinking, as the warm/cold air boundary shifts northward in this phase. Wrona and Rohli (2007) found no strong evidence at the monthly scale for a link between the AO or NAO and R_c.

The Pacific-North American (PNA) pattern is another important component of mid-latitude flow, consisting of anomalies in the geopotential height fields (typically at 700 or 500 hPa) observed over the western and eastern United States (Wallace & Gutzler, 1981). The positive phase consists of above-normal geopotential heights (i.e., ridging) over western North America and below normal geopotential heights (i.e., troughing) over the eastern United States, allowing cold Canadian air to plunge southeastward, resulting in negative

temperature anomalies over the eastern United States and positive temperature anomalies over western North America (Leathers & Palecki, 1992; Leathers et al., 1991). The negative phase features troughing or at least negative height departures over western North America, and simultaneous ridging or positive height departures over the eastern United States, resulting in negative temperature departures in the western mountain cordillera and positive temperature departures over the eastern United States (Leathers & Palecki, 1992). The PNA pattern has been found to be strongly influenced by ENSO (Renwick & Wallace, 1996; Straus & Shukla, 2002; C. Wang et al., 2020), with the positive (negative) phase of the PNA pattern tending to be associated with Pacific warm (cold) episodes (i.e., El Niño [La Niña]). The cumulative effect of the NAO and PNA pattern acting in concert can amplify U.S. temperature anomalies (Baxter & Nigam, 2013; Ning & Bradley, 2016; Notaro et al., 2006). Burnett (1993) found that the increased frequency of the positive mode of the PNA pattern may have supported a temporal increase in NHCPV area from the mid-1960s to the mid-1980s, largely because of amplified troughing over the central Pacific Ocean and eastern North America/Atlantic Ocean. Not surprisingly, because of its amplified ridge-trough configuration in its positive mode, the PNA pattern is negatively correlated to NHCPV R_c in December, January, and to some extent, October (Bushra & Rohli, 2019; Wrona & Rohli, 2007).

Although a substantial number of studies has been carried out to demonstrate the relationship between variability in teleconnection indices and atmospheric variables at climatological time scales, none have included the CPV. Given that other studies show significant associations of teleconnections to surface meteorological anomalies, other teleconnections are likely to be linked to NHCPV variability. However, some may have compensating effects across longitudes, yielding no significant net change in NHCPV area or circularity. Others, such as the Pacific Decadal Oscillation (PDO; Newman et al., 2003) are potentially useful but do not have indices that are available on a daily basis. And some indices of teleconnections, particularly those representing ENSO, are unavailable on a daily basis even though daily data exist for other indices of that teleconnection (e.g., Multivariate ENSO index; Wolter & Timlin, 2011). Therefore, the present research is needed to ascertain whether the linkage between the NHCPV area and/or R_c and the SOI, Niño3.4, NAO, AO, and PNA appear at the daily scale using the "steepest gradient" approach, and at all months rather than only those in winter and one representative month of each season as tested in Bushra and Rohli (2019). This issue is important to address because the size and shape of the CPV is inherently tied to the locations of baroclinicity and upper-level support for surface systems associated with impactful extreme weather.

3. Materials and Methods

Statistically standardized daily atmospheric teleconnection index data are downloaded from URLs shown in Bushra and Rohli (2019; their Table 1). To facilitate comparison of results with that of the previous study, NHCPV area and R_c are calculated from geopotential height data from the National Centers for Environmental Prediction/National Center for Atmospheric Research (NCEP/NCAR; Kanamitsu et al., 2002). Also as in Bushra and Rohli (2019), the leading edge of the CPV is defined by connecting the points representing the steepest gradient of 500-hPa geopotential height along each longitude, daily from 1979 to 2017. NHCPV area is calculated after projecting the polygon using Lambert's equal area projection. R_c is defined as in Bushra and Rohli (2019), using the conformal polar stereographic projection. Delineating the daily CPV involves resolving the computational challenges of preserving complicated shapes that appear in the daily data but get "washed out" in monthly mean data, namely perforations such as cutoff lows of colder air surrounded spuriously by warmer air and narrow zones of colder air equatorward of warmer air.

Daily mean teleconnection indices for the NAO, AO, and PNA pattern in the satellite era beginning in 1979 and for the SOI and Niño3.4 since 1991 and 1990, respectively, are used. These time periods are selected to match the periods for which the NHCPV area and R_c were computed by Bushra and Rohli (2019). For each time period, a Pearson product-moment correlation matrix is calculated between the daily NHCPV area and R_c, with the five standardized indices representing the four teleconnections. To ensure an adequate number of observations while still remaining true to the mission of representing daily variability accurately, the NHCPV area and (separately) R_c are standardized daily (by subtracting the mean for that Julian day and then dividing by the standard deviation for that Julian day) over the 1979 to 2017 period, while the teleconnections are standardized using all data available between 1979 and 2017.

Table 1
Pearson Product-Moment Correlations of the Area and Circularity Ratio (R_c) of the Northern Hemisphere's Circumpolar Vortex Versus Atmospheric and Sea Surface Temperature Indices, at the Daily Time Scale, for the Periods of Available Records of Teleconnection Indices (January 1979 to September 2017 for the AO, NAO, and PNA Pattern, January 1991 Through December 2017 for the SOI, and January 1990 Through December 2017 for the Niño3.4)

	Area					R_c				
Month	AO	NAO	PNA	SOI	Niño3.4	AO	NAO	PNA	SOI	Niño3.4
January	**−0.068**	**0.084**	−0.034	0.024	0.043	**0.132**	0.014	**−0.187**	**0.101**	**−0.144**
	0.018	**0.003**	0.242	0.502	0.202	**<0.001**	0.626	**<0.001**	**0.004**	**<0.001**
February	−0.040	**0.110**	−0.047	0.027	0.049	**0.127**	−0.012	**−0.221**	0.006	**−0.089**
	0.183	**<0.001**	0.119	0.461	0.169	**<0.001**	0.699	**<0.001**	0.878	**0.012**
March	**−0.196**	**−0.138**	0.012	0.055	−0.002	**0.199**	**0.101**	**−.0.242**	−0.040	−0.044
	<0.001	**<0.001**	0.678	0.119	0.944	**<0.001**	**<0.001**	**<0.001**	0.256	0.192
April	**−0.332**	**−0.057**	**0.115**	−0.006	0.040	**0.273**	**0.110**	**−0.204**	0.022	−0.006
	<0.001	**0.050**	**<0.001**	0.873	0.251	**<0.001**	**<0.001**	**<0.001**	0.546	0.867
May	**−0.315**	**−0.108**	**0.104**	−0.016	**−0.073**	**0.239**	**0.069**	**−0.221**	0.061	−0.001
	<0.001	**<0.001**	**<0.001**	0.640	**0.030**	**<0.001**	**0.017**	**<0.001**	0.086	0.980
June	**−0.301**	**−0.262**	**0.079**	−0.116	0.021	**0.232**	**0.184**	**−0.130**	0.058	−0.016
	<0.001	**<0.001**	**<0.001**	<0.001	0.541	**<0.001**	**<0.001**	**<0.001**	0.097	0.653
July	**−0.326**	**−0.181**	**0.155**	−0.024	**0.166**	**0.246**	**0.129**	**−0.175**	0.066	**−0.128**
	<0.001	**<0.001**	**<0.001**	0.490	**<0.001**	**<0.001**	**<0.001**	**<0.001**	0.057	**<0.001**
August	**−0.237**	**0.062**	**0.448**	−0.020	−0.016	**0.202**	−0.020	**−0.270**	−0.001	0.024
	<0.001	**0.030**	**<0.001**	0.569	0.634	**<0.001**	0.479	**<0.001**	0.987	0.478
September	**−0.247**	−0.055	**0.227**	**0.192**	**−0.245**	**0.197**	−0.006	**−0.170**	**−0.152**	**0.195**
	<0.001	0.061	**<0.001**	**<0.001**	**<0.001**	**<0.001**	0.838	**<0.001**	**<0.001**	**<0.001**
October	**−0.213**	**−0.139**	0.034	**−0.099**	−0.048	0.242	**0.117**	**−0.144**	**0.079**	0.0286
	<0.001	**<0.001**	0.233	**0.004**	0.161	<0.001	**<0.001**	**<0.001**	**0.022**	0.399
November	**−0.261**	**−0.098**	**0.138**	0.062	**−0.088**	**0.307**	**0.179**	**−0.276**	−0.047	0.036
	<0.001	**<0.001**	**<0.001**	0.077	**0.010**	**<0.001**	**<0.001**	**<0.001**	0.180	0.293
December	**−0.167**	0.055	**0.176**	**0.110**	**−0.099**	**0.170**	−0.0155	**−0.222**	−0.050	0.040
	<0.001	0.055	**<0.001**	**0.001**	**0.003**	**<0.001**	0.590	**<0.001**	0.151	0.241

Note. Correlations significant at $\alpha \leq 0.05$ are shown in bold.

AO, Arctic Oscillation; NAO, North Atlantic Oscillation; PNA, Pacific-North American; SOI, Southern Oscillation index.

Because the position and amplitude of the NHCPV's ridges and troughs may not necessarily be associated with NHCPV area (i.e., the ridges and troughs could simply progress or retrogress, or amplify in some places and dampen simultaneously in others), and because the ridges and troughs progress and retrogress temporally, it is important to identify the teleconnections that, individually or collectively, may vary coincidentally with CPV area and/or CPV R_c. Thus, PCA is applied to identify trends in the main modes of holistic spatio-temporal variability of the relationships between the NHCPV and the teleconnections (Demšar et al., 2013).

PCA is one of the oldest and most popular dimensionality reduction methods applied in the atmospheric sciences, operating by identifying common patterns within a data set by linearly transforming the original data to new dimensions that explain successively less data set variability (Jackson, 2005). As such, PCA is useful for illustrating the teleconnection/CPV relationship, in which broad-scale dynamics are inferred from inspection of patterns resulting (primarily) from PCA, through space and time simultaneously. To date, PCA has been used in atmospheric research such as in identifying and assessing analog forecasting

Table 2
Pearson Product-Moment Correlation Matrix and p-Values of the Daily Northern Hemisphere's Circumpolar Vortex Metrics and Teleconnection Indices, for the Available Periods of Record Indicated in Table 1

Variable	Area	R_c	AO	NAO	PNA	SOI
R_c	−0.528**					
AO	−0.141**	0.383**				
NAO	−0.012	0.210**	0.551**			
PNA	0.132**	−0.268**	−0.147**	0.046**		
SOI	0.012	0.044**	0.048**	0.031*	−0.069**	
Niño3.4	−0.028*	−0.049**	−0.016	0.016	0.066**	−0.469**

Note. *$p < 0.05$ **$p < 0.01$.
AO, Arctic Oscillation; NAO, North Atlantic Oscillation; PNA, Pacific-North American; SOI, Southern Oscillation index.

(Grimmer, 1963), spatial variability (e.g., Kutzbach, 1967; Stidd, 1967), classification (e.g., Dyer, 1975) and regionalization (e.g., Comrie & Glenn, 1998; Mallants & Feyen, 1990; Richman & Lamb, 1985), and circulation changes (e.g., Compagnucci & Vargas, 1998).

Feldstein (2000) implemented PCA in examining the daily ENSO, NAO, PNA, and west Pacific (Barnston & Livezey, 1987; Wallace & Gutzler, 1981) teleconnection timescale, power spectra, and climate noise properties from the unfiltered 300-hPa geopotential height field. McCabe and Dettinger (2002) used PCA to analyze snowpack variability associated with atmospheric teleconnections in the western United States. Sobolowski and Frei (2007) employed PCA to characterize the relationship between North American winter snow mass and the SOI/Niño3.4, NAO, PNA, and PDO indices. Lopez-Bustins et al. (2008) examined the spatial distribution of precipitation trends on the Iberian Peninsula in relation to the AO, NAO, and Western Mediterranean Oscillation (Dünkeloh & Jacobeit, 2003) and surface circulation patterns identified with PCA. Hatzaki et al. (2007) applied PCA on a seasonal and monthly basis on daily NCEP/NCAR geopotential heights data to identify teleconnection influences on atmospheric circulation, centered over eastern Mediterranean.

In this research, an input matrix consisting of seven columns (i.e., the five daily standardized teleconnection indices and the two daily standardized indices of the NHCPV [i.e., area and R_c]) and 9,705 rows (i.e., month/day/year), is input into a P-mode PCA data structure (Richman, 1986). The correlation matrix of the seven daily standardized variables against each other is then produced, with the loadings matrix output consisting of the seven variables along the rows versus the first seven principal components. The output component scores matrix, by principal component (columns) versus time (rows) allows for detailed analysis of the time series of changes in the atmospheric configuration consisting of the teleconnections and NHCPV properties. Then, 16 additional, separate PCAs are run on the same daily standardized data, for each of the 12 months and for each meteorological season (D-J-F, M-A-M, J-J-A, and S-O-N), to identify the extent of consistency and aid in explanation of forcing features.

While the standardization process satisfies the PCA assumption of non-stationarity in the seasonality of the atmospheric data, the Durbin-Watson (D-W) test (Savin & White, 1977) is used to assess the validity of the assumption of the absence of serial autocorrelation (Vanhatalo & Kulahci, 2016). A D-W test statistic of 0–4 is output, whereby values above (below) 2 suggest (negative) positive autocorrelation, mostly applicable for time series data. According to Field (2009), values below 1

Table 3
Durbin-Watson Test and p-Value for the First-Order Autoregressive Process

Variable	Before C-O procedure	After C-O procedure
Area	1.91	1.993
R_c	1.974	1.997
AO	0.884	1.990
NAO	0.905	1.894
PNA	1.738	[a]Did not converge
SOI	1.682	[a]Did not converge
Niño3.4	0.351	2.034

[a]An iterative approach continues until there is convergence in calculating the regression coefficients.
AO, Arctic Oscillation; C-O, Cochrane-Orcutt; NAO, North Atlantic Oscillation; PNA, Pacific-North American; SOI, Southern Oscillation index.

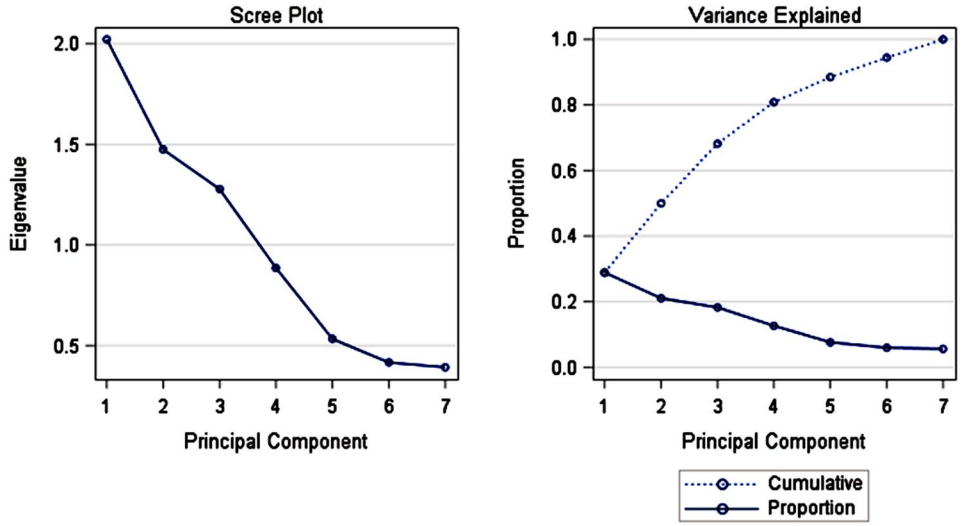

Figure 1. Scree plot showing (a) eigenvalue and (b) proportion and cumulative proportion of the explained variability, by principal component, using available periods of record for the seven variables as described in Table 1.

or exceeding 3 could be cause for concern. The Cochrane-Orcutt (C-O) method (Montgomery et al., 2012) is used to remove any such autocorrelation.

4. Results

4.1. Pearson Correlation Analysis

Pearson correlations are calculated at the daily scale between NHCPV area (and separately, R_c) versus each of the five teleconnection indices, for each of the 12 months, as was done in Bushra and Rohli (2019). A greater number of statistically significant correlations occurred between NHCPV area and (separately) R_c versus the teleconnection indices at the daily scale than Bushra and Rohli (2019) reported at the monthly scale. Specifically, 37 (38) statistically significant (although not necessarily practically significant) correlations, or 61.67% (63.33%) of the pairs of variables, for CPV area (R_c) exist, respectively (Table 1). These numbers compare to 18 (27), or 30.0% (45.0%), as shown in Table 3 from Bushra and Rohli (2019) for the same teleconnections and study period, but for monthly data. It should be noted that the PDO was analyzed at the monthly scale by Bushra and Rohli (2019), but this teleconnection was not analyzed here because daily values were unavailable. However, the relatively low explained variance for some correlations suggests that caution should be exercised in the interpretation of results.

Table 1 reveals many interesting patterns. As was the case at the monthly scale, the AO shows the strongest relationship among the teleconnection indices to both NHCPV area and R_c. The AO is correlated significantly to both area (negatively) and R_c (positively) in 11 of the 12 months, with February having a significant correlation only to R_c. Also expectedly similar to the work at the monthly scale, the daily NAO is linked in largely the same manner as the AO, with a positive NAO index associated with a significantly anomalously small and circular NHCPV, but only in seven months each for area and R_c. The NAO's linkage to the NHCPV weakens or even reverses in winter, a finding that was largely supported in previous monthly scale analysis (Bushra & Rohli, 2019), perhaps owing to the NAO's regional scope versus the NHCPV's hemispheric scope. The daily PNA pattern has a significantly positive link to NHCPV area in eight months, with a weaker association in winter, and a negative link to R_c in all months. The two ENSO indices correlate more weakly with NHCPV and R_c, though they are still statistically significant in some months, as compared to the three indices of extratropical teleconnections.

Daily NHCPV area is inversely associated with R_c, and several of the daily teleconnection indices are correlated with each other (Table 2). For example, it is not surprising that strongly significant positive relationships exist between the AO and NAO, and significant negative relationships exist between SOI and Niño3.4.

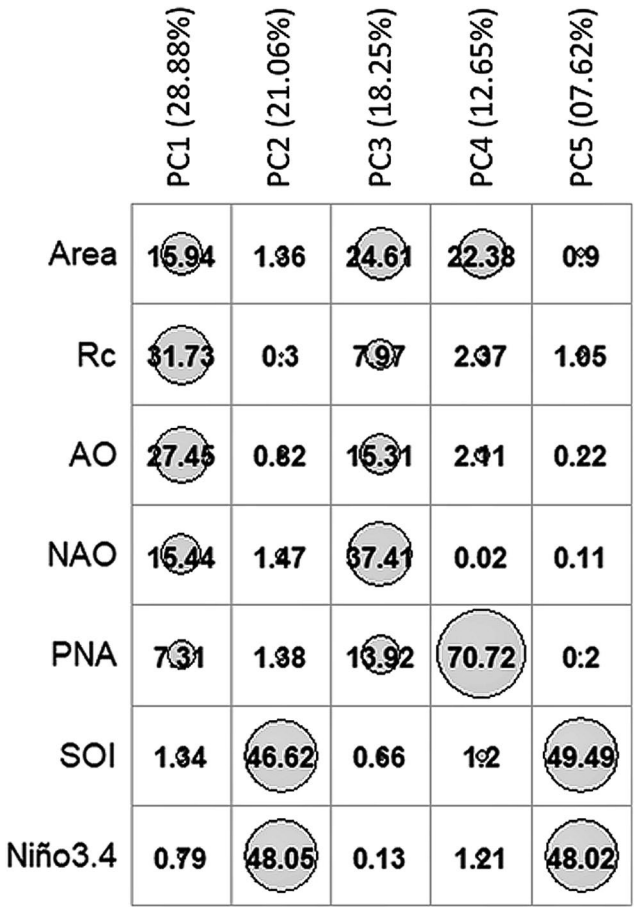

Figure 2. Percentage of total variance explained by each of the first five PCs by Northern Hemisphere circumpolar vortex (NHCPV) area, NHCPV circularity ratio (R_c), and five atmospheric teleconnection indices, for the period of record designated in Table 1. The numerals in parentheses across the columns indicate the total percentage of data set variance explained by the PCs.

Overall daily correlations across all months verify the results in Table 1, with even the tropical teleconnections showing evidence for linkages to the NHCPV. A surprising result is the positive correlation between NAO and PNA pattern, which contradicts past research (Pinto et al., 2011) and the NAO versus AO correlation. It is possible that the observed lag with the NAO leading the PNA of opposite sign (Baxter & Nigam, 2013) may explain the positive, non-lagged relationship found here. In general, the association between variables calls for PCA to identify the main modes of data set variability independently of these associations.

4.2. Durbin-Watson and Cochrane-Orcutt Tests

Because teleconnections tend to change relatively slowly over time, it is not surprising that the D-W test on daily teleconnection indices (and CPV area and R_c affected by them) reveals the existence of serial correlation for the first-order autoregressive process. However, much reduced values of the D-W statistic result for the AO, NAO, and Niño3.4 after applying the C-O procedure (Table 3). Although the PNA pattern index and SOI did not converge (which is a continuation of an iterative approach until calculating the regression coefficients, ρ) after applying the C-O adjustment, they were input into the PCA before applying the C-O procedure since the original D-W test statistics fell within the range of 1.5–2.5.

4.3. Principal Components Analysis (PCA)

The first PC explains nearly 29% of the data set variance, while the first three components explain more normalized variance than the original variables that compose them, as indicated by their eigenvalues that exceed 1.0. A scree plot (Jackson, 2005) in Figure 1 suggests that the first five components, which collectively explain almost 90 percent of the data set variability, should be examined more closely. This approach accomplishes the goal of data reduction, to identify the main modes of variability in the data set, so that intercorrelations among the different teleconnections and CPV area and R_c are removed.

The explained variance by principal component (Figure 2) shows that R_c is the most strongly represented variable in PC1, while PCs 2 and 5 capture the ENSO indices most effectively. PC3 best represents the NAO with strong representation of both NHCPV area and the NAO-related AO. PC4 is the "PNA pattern" component.

The PCA-generated eigenvalues for individual months and seasons suggest that a relatively consistent relationship among the variables across the monthly and seasonal time scales exists (Table 4). Moreover, similar patterns of prominence of R_c, ENSO, NAO, and PNA in PCs 1 through 4, respectively, persist in general in each season (Figure 3), verifying the robustness of the results. In every case, approximately 80% of the variance is explained by the four PCs, but differences from month to month for PC1 and PC2 are noteworthy, as indicated by eigenvalues that exceed 1.0 (Table 4). Specifically, PC1 is slightly less important in late winter/early spring than at most other times of the year while PC2 is more important, and other months have complimentary explained variance for these two components (Figure 4). Similar complimentary patterns are apparent between PC3 and PC4 but with less explained variability. Not surprisingly, the ENSO-dominated PC2 shows less prominence in April through July (Figure 4), which overlaps substantially with a time when ENSO has its weakest signature.

The PCA-generated scores matrix provides a time series of influence of the various PCs. Linear tests for trend suggest that PC3 is weakening significantly over time ($p < 0.001$), while PCs 4 and 5 are strengthening temporally ($p < 0.001$; Figure 5). PCs 1, 2, 6, and 7 show no significant linear temporal trend.

Table 4
Proportion of Variability, and Cumulative Percentage, Explained by the First Four Principal Components, in Principal Components Analysis by Month and Meteorological Season (D-J-F, M-A-M, J-J-A, and S-O-N), for Daily Northern Hemisphere Circumpolar Vortex (NHCPV) Area, NHCPV Circularity Ratio (R_c), and the Five Atmospheric Teleconnection Indices, for the Period of Record Designated in Table 1

	PC1		PC2		PC3		PC4	
	Eigenvalue		Eigenvalue		Eigenvalue		Eigenvalue	
	Prop	Cumul	Prop	Cumul	Prop	Cumul	Prop	Cumul
January	2.296		1.481		1.356		0.767	
	0.328	0.328	0.212	0.540	0.194	0.733	0.110	0.843
February	2.058		1.633		1.325		0.912	
	0.294	0.294	0.233	0.527	0.189	0.717	0.130	0.847
March	1.981		1.725		1.179		0.886	
	0.283	0.283	0.246	0.529	0.168	0.698	0.127	0.824
April	2.218		1.448		1.218		0.753	
	0.317	0.317	0.207	0.524	0.174	0.698	0.108	0.805
May	2.224		1.295		1.152		0.890	
	0.318	0.318	0.185	0.503	0.165	0.667	0.127	0.795
June	2.413		1.363		0.993		0.920	
	0.345	0.345	0.195	0.540	0.142	0.681	0.132	0.813
July	2.282		1.414		1.197		0.736	
	0.326	0.326	0.202	0.528	0.171	0.699	0.105	0.804
August	2.356		1.569		1.271		0.649	
	0.337	0.337	0.224	0.561	0.182	0.742	0.093	0.835
September	2.080		1.502		1.219		0.835	
	0.297	0.297	0.215	0.512	0.174	0.686	0.119	0.805
October	2.184		1.573		1.140		0.878	
	0.312	0.312	0.225	0.537	0.163	0.700	0.126	0.825
November	2.351		1.434		1.078		0.895	
	0.336	0.336	0.205	0.541	0.154	0.695	0.128	0.823
December	1.984		1.664		1.400		0.765	
	0.283	0.283	0.238	0.521	0.200	0.721	0.109	0.830
Winter	2.030		1.542		1.421		0.841	
	0.290	0.290	0.220	0.510	0.203	0.713	0.120	0.833
Spring	2.058		1.499		1.168		0.843	
	0.294	0.294	0.214	0.508	0.167	0.675	0.120	0.800
Summer	2.276		1.400		1.209		0.792	
	0.325	0.325	0.200	0.525	0.173	0.698	0.113	0.811
Autumn	2.072		1.568		1.175		0.876	
	0.296	0.296	0.224	0.520	0.168	0.688	0.125	0.813

5. Discussion

5.1. Teleconnection Analysis

The increased number of significant correlations at the daily scale, as compared to the monthly scale in previous work, suggests that monthly analyses may "wash out" some of the sub-monthly-scale variability that links atmospheric flow and NHCPV properties. The finding that the extratropical teleconnections

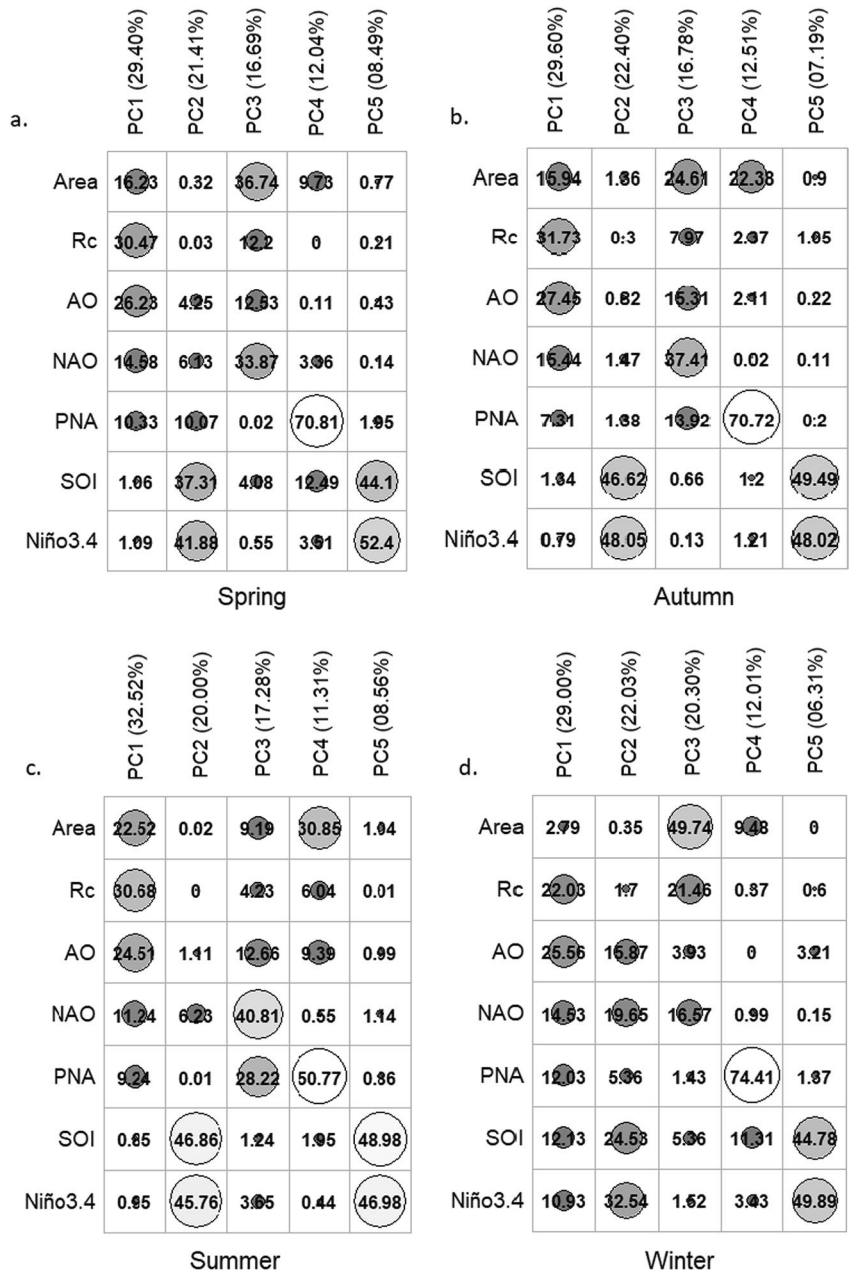

Figure 3. As in Figure 2, but by meteorological season (a) D-J-F, (b) M-A-M, (c) J-J-A, and (d) S-O-N.

(NAO, AO, PNA) can influence the daily NHCPV variability is important, because most impactful weather phenomena in the extratropics are related to upper-level support that is represented by CPV behavior.

The finding that NHCPV area is inversely related to the daily AO index in all months except February comes as no surprise, as the positive AO index is linked to a poleward retreat of the polar front (Budikova, 2008). The finding of a strongly positive association between R_c and the AO in every month at the daily scale confirms that the areal retreat is tied to zonal flow in the positive phase (Thompson & Wallace, 2000) and meridional (i.e., wavy) flow in the negative phase (Shi et al., 2021). The similarity of associations between the regional expression of the AO—the NAO—and the NHCPV, with positive (negative) NAO tied to small and more circular NHCPV, corroborates these findings. In contrast, studies based on the observational record have found decreased Northern Hemisphere zonality in past decades associated with warming (Cattiaux

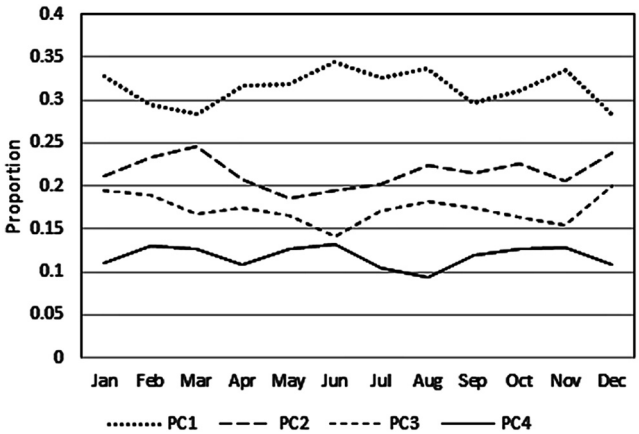

Figure 4. Proportion of variability explained by the first five principal components, by month, for the patterns representing the interconnections between daily Northern Hemisphere circumpolar vortex (NHCPV) area, NHCPV circularity ratio (R_c), and the five atmospheric teleconnection indices, for the period of record designated in Table 1.

et al., 2016), and decreased zonality during autumn and summer over North America albeit amid a general increase in zonality during summer (Di Capua & Coumou, 2016).

Our finding regarding NHCPV area and R_c tendencies could shed light in the ongoing debate over the role of Arctic amplification in driving changes to the mid-latitude steering flow (Holland & Bitz, 2003; Pithan & Mauritsen, 2014) by supporting the assertion of Cattiaux et al. (2016) that increased zonality is to be expected under future warming conditions. More specifically, our result suggests, albeit indirectly, that an increasingly positive AO index might affect the transfer of energy from the tropics to the poles in both the atmosphere (e.g., Cohen et al., 2014) and ocean (e.g., Praetorius, 2018; Rahmstorf et al., 2015), but Cohen et al. (2018) suggested that increasing severe weather might accompany the negative AO. But on the other hand, Arctic amplification may also impact the circularity of the NHCPV by weakening the zonal winds, including in the lower stratosphere in winter (Kretschmer et al., 2018), in part because of non-uniform warming rates by latitude, which may be connected to changes in Rossby wave activity. Francis and Vavrus (2012, 2015) suggested that amplified waviness is more likely in the future as a result of these weakened zonal winds. Despite the fact that our results here tend to favor the suggestion of Cattiaux et al. (2016), further work must be done to ascertain more clearly the most likely scenario, as Vavrus (2018) summarized the conflicting evidence and lamented the continuing lack of consensus. Our work is but one piece of a complicated puzzle.

It is also not surprising that the amplified ridge-trough configuration over mid-latitude North America captured by the positive mode of the PNA pattern is linked to an anomalously enlarged and less circular NHCPV. The implication is that an expanded pool of polar air in the Northern Hemisphere is associated with meridionality over North America and a smaller pool of polar air is linked to zonality over North America. However, the fact that this linkage is weaker in winter is somewhat surprising and is perhaps explained by the importance of other factors, namely the variability in extent and position of Eurasian snow cover as a driver of the winter NHCPV area and circularity. In general, these results support the findings at the monthly scale reported by Bushra and Rohli (2019).

5.2. PCA

The PCA procedure confirms the close association between the NHCPV area and the AO and NAO through space and time. The temporal weakening of PC3 (the NAO component) may suggest that this teleconnection is becoming less dominant than the AO regarding NHCPV area and R_c. On the other hand, the increasing role of two components that explain lesser variance (the PNA pattern and the second ENSO pattern) implies that these may have become more prominent players in recent years, including, perhaps, as drivers of the NHCPV area and R_c. The latter implication contradicts findings of Cohen (2016), who found weakened tropical forcing due to ENSO in recent decades. One possible explanation is that a blurring of the lines delineating the NHCPV (i.e., weakening if the NHCPV) as the poles continue to warm at faster rates than the tropics may allow for more meandering of the leading edge of the NHCPV (Kretschmer et al., 2018), leading to ridge amplification in the region of the Pacific and western North America and increased influence of tropical Pacific air-sea variability.

The complementarity of the PCA time series between PC1 and PC2 (Figure 4), along with the data in Table 2, suggest that a near-circular NHCPV is related to the La Niña phase of ENSO, while a wavy NHCPV is linked to the El Niño phase. This connection was noticed by Frauenfeld and Davis (2000) who identified an expanded extratropical circulation over the Pacific and contracted circumpolar vortex over western North America (reminiscent of the positive PNA pattern) during the El Niño phase, with opposite and weaker impacts in La Niña. Furthermore, Frauenfeld and Davis (2000) noted the importance of identifying ENSO based on SST for capturing the continuity of the warm pool associated with the El Niño phase, suggesting

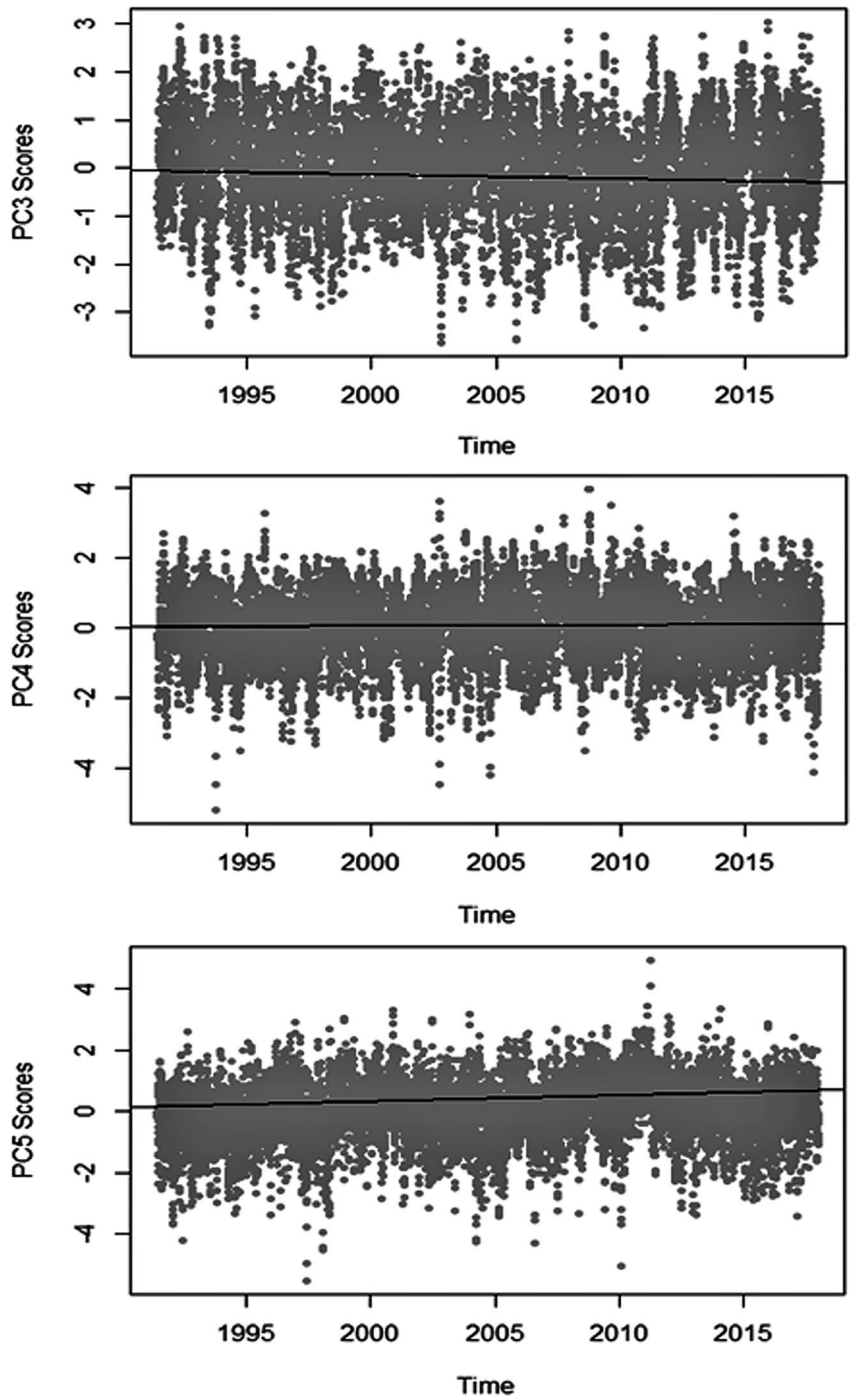

Figure 5. Significant linear temporal trends in daily principal components analysis-generated scores for PCs 3, 4, and 5.

ENSO-related tropical forcing of the mid-latitudes, rather than mid-latitude forcing of the tropics. Nevertheless, the relatively weak association between ENSO and the NHCPV (Table 1) largely corroborates the results of Straus and Shukla (2002), who suggested that El Niño phase does not force the PNA pattern, and that the La Niña phase was inconclusive in its influence of the PNA pattern. The complementarity between PC3 and PC4 (Figure 4) confirms the intuitive oscillation of importance between the NAO and PNA, with zonal flow associated with the NAO tied to the negative PNA index, and meridional NAO flow linked to a

positive PNA, despite the fact that this linkage is not revealed through simple correlation of the two indices (Table 2). The fact that the relative influence of the PCs on data set variability remains largely consistent throughout the year suggests that the CPV/teleconnection relationship is important in all months.

6. Summary and Conclusion

This research assesses the linkages between the atmospheric teleconnections and the NHCPV area and R_c. Results suggest that both NHCPV area and R_c are more strongly correlated with the extratropical AO, NAO, and PNA teleconnections than with the tropical ENSO phenomenon. Most notably, the warm (i.e., positive) phase of the AO, which dominates the latter part of the study period, is tied to an anomalously small and circular NHCPV. The PCA suggests that NHCPV R_c is closely tied to the PC dominated by the AO and NAO, acting together. Results also point to a linkage between NHCPV area and the component dominated by the PNA teleconnection. These results represent a step forward in using predicted or observed high-frequency shifts in the teleconnection indices to anticipate potential extreme events at short lead times.

Future work should investigate the vertical consistency of these results, so that inferences can be drawn about whether changes in height of the NHCPV over time in response to surface warming might be confounding results shown here. Furthermore, the reduced amplitudes of the Rossby waves in the Southern Hemisphere as compared to those in the Northern Hemisphere might call for a more precise and sensitive method of evaluating daily variability and long-term changes in the Southern Hemispheric CPV, such as the method proposed by Bushra and Rohli (2019) employed here. An analysis of the degree of synchronicity of anomalies in area and circularity of the two CPVs could shed light on the cross-hemisphere influence of the teleconnections. In general, improvements in our understanding of the CPVs, at both the daily and monthly time scales, may identify signatures that might provide a harbinger of abrupt, impactful weather and climate events and impacts of longer-term climatic changes.

Data Availability Statement

The gridded data set was obtained from the National Centers for Environmental Prediction (NCEP)/Department of Energy (DOE) Reanalysis 2 project. The data are available at https://www.esrl.noaa.gov/psd/data/gridded/data.ncep.reanalysis2.pressure.html.

Acknowledgments
The authors are grateful for funding from the Louisiana State University Economic Development Assistantship Program and the Dissertation Year Fellowship program. Methods associated with the generation of the data used in this research to characterize the NHCPV properties (i.e., CPV centroid location, area, and circularity), are described in more detail in Bushra and Rohli (2019).

References

Ambaum, M. H., Hoskins, B. J., & Stephenson, D. B. (2001). Arctic oscillation or North Atlantic oscillation? *Journal of Climate*, *14*(16), 3495–3507. https://doi.org/10.1175/1520-0442(2001)014<3495:aoonao>2.0.co;2

Angell, J. K. (1992). Relation between 300-mb north polar vortex and equatorial SST, QBO, and sunspot number and the record contraction of the vortex in 1988-89. *Journal of Climate*, *5*(1), 22–29. https://doi.org/10.1175/1520-0442(1992)005<0022:rbmnpv>2.0.co;2

Angell, J. K. (2001). Relation of size and displacement of the 300 mbar north circumpolar vortex to QBO, El Niño, and sunspot number, 1963–2000. *Journal of Geophysical Research*, *106*(D23), 31787–31794. https://doi.org/10.1029/2001JD000473

Angell, J. K., & Korshover, J. (1977). Variation in size and location of 300 mb north circumpolar vortex between 1963 and 1975. *Monthly Weather Review*, *105*(1), 19–25. https://doi.org/10.1175/1520-0493(1977)105<0019:visalo>2.0.co;2

Barnston, A. G., & Livezey, R. E. (1987). Classification, seasonality and persistence of low-frequency atmospheric circulation patterns. *Monthly Weather Review*, *115*(6), 1083–1126. https://doi.org/10.1175/1520-0493(1987)115<1083:csapol>2.0.co;2

Baxter, S., & Nigam, S. (2013). A subseasonal teleconnection analysis: PNA development and its relationship to the NAO. *Journal of Climate*, *26*(18), 6733–6741. https://doi.org/10.1175/JCLI-D-12-00426.1

Budikova, D. (2008). Effect of the Arctic Oscillation on precipitation in the eastern USA during ENSO winters. *Climate Research*, *37*(1), 3–16. https://doi.org/10.3354/cr00749

Burnett, A. W. (1993). Size variations and long-wave circulation within the January northern-hemisphere circumpolar vortex - 1946–89. *Journal of Climate*, *6*(10), 1914–1920. https://doi.org/10.1175/1520-0442(1993)006<1914:svalwc>2.0.co;2

Bushra, N., & Rohli, R. V. (2019). An objective procedure for delineating the circumpolar vortex. *Earth and Space Science*, *6*(5), 774–783. https://doi.org/10.1029/2019EA000590

Cattiaux, J., Peings, Y., Saint-Martin, D., Trou-Kechout, N., & Vavrus, S. J. (2016). Sinuosity of midlatitude atmospheric flow in a warming world. *Geophysical Research Letters*, *43*(15), 8259–8268. https://doi.org/10.1002/2016GL070309

Clarke, A. J., & van Gorder, S. (2001). ENSO prediction using an ENSO trigger and a proxy for western equatorial Pacific warm pool movement. *Geophysical Research Letters*, *28*(4), 579–582. https://doi.org/10.1029/2000GL012201

Cohen, J. (2016). An observational analysis: Tropical relative to Arctic influence on midlatitude weather in the era of Arctic amplification. *Geophysical Research Letters*, *43*(10), 5287–5294. https://doi.org/10.1002/2016GL069102

Cohen, J., Pfeiffer, K., & Francis, J. A. (2018). Warm Arctic episodes linked with increased frequency of extreme winter weather in the United States. *Nature Communications*, *9*(1), 1–12. https://doi.org/10.1038/s41467-018-02992-9

Cohen, J., Screen, J. A., Furtado, J. C., Barlow, M., Whittleston, D., Coumou, D., et al. (2014). Recent Arctic amplification and extreme mid-latitude weather. *Nature Geoscience*, *7*(9), 627–637. https://doi.org/10.1038/NGEO2234

Compagnucci, R. H., & Vargas, W. M. (1998). Inter-annual variability of the Cuyo rivers' streamflow in the Argentine-an Andean mountains and ENSO events. *International Journal of Climatology*, *18*(14), 1593–1609. https://doi.org/10.1002/(sici)1097-0088(19981130)18:14<1593::aid-joc327>3.0.co;2-u

Comrie, A. C., & Glenn, E. C. (1998). Principal components-based regionalization of precipitation regimes across the southwest United States and northern Mexico, with an application to monsoon precipitation variability. *Climate Research*, *10*(3), 201–215. https://doi.org/10.3354/cr010201

Demšar, U., Harris, P., Brunsdon, C., Fotheringham, A. S., & McLoone, S. (2013). Principal component analysis on spatial data: An overview. *Annals of the Association of American Geographers*, *103*(1), 106–128. https://doi.org/10.1080/00045608.2012.689236

Deser, C., & Blackmon, M. L. (1993). Surface climate variations over the North Atlantic Ocean during winter: 1900–1989. *Journal of Climate*, *6*(9), 1743–1753. https://doi.org/10.1175/1520-0442(1993)006<1743:scvotn>2.0.co;2

Di Capua, G., & Coumou, D. (2016). Changes in meandering of the Northern Hemisphere circulation. *Environmental Research Letters*, *11*(9), 094028. https://doi.org/10.1088/1748-9326/11/9/094028

Dünkeloh, A., & Jacobeit, J. (2003). Circulation dynamics of Mediterranean precipitation variability 1948–98. *International Journal of Climatology*, *23*(15), 1843–1866. https://doi.org/10.1002/joc.973

Dyer, T. G. J. (1975). The assignment of rainfall stations into homogeneous groups: An application of principal component analysis. *Quarterly Journal of the Royal Meteorological Society*, *101*(430), 1005–1013. https://doi.org/10.1002/qj.49710143020

Feldstein, S. B. (2000). The timescale, power spectra, and climate noise properties of teleconnection patterns. *Journal of Climate*, *13*(24), 4430–4440. https://doi.org/10.1175/1520-0442(2000)013<4430:ttpsac>2.0.co;2

Field, A. (2009). *Discovering statistics using SPSS* (3rd ed.). Sage.

Francis, J. A., & Vavrus, S. J. (2012). Evidence linking Arctic amplification to extreme weather in mid-latitudes. *Geophysical Research Letters*, *39*(6), L06801. https://doi.org/10.1029/2012GL051000

Francis, J. A., & Vavrus, S. J. (2015). Evidence for a wavier jet stream in response to rapid Arctic warming. *Environmental Research Letters*, *10*(1), 014005. https://doi.org/10.1088/1748-9326/10/1/014005

Frauenfeld, O. W., & Davis, R. E. (2000). The influence of El Niño-Southern Oscillation events on the Northern Hemisphere 500 hPa circumpolar vortex. *Geophysical Research Letters*, *27*(4), 537–540. https://doi.org/10.1029/1999GL010996

Frauenfeld, O. W., & Davis, R. E. (2003). Northern Hemisphere circumpolar vortex trends and climate change implications. *Journal of Geophysical Research*, *108*(D14), 4423. https://doi.org/10.1029/2002JD002958

Grimmer, M. (1963). The space-filtering of monthly surface temperature anomaly data in terms of pattern, using empirical orthogonal functions. *Quarterly Journal of the Royal Meteorological Society*, *89*(381), 395–408. https://doi.org/10.1002/qj.49708938111

Hardiman, S. C., Dunstone, N. J., Scaife, A. A., Smith, D. M., Ineson, S., Lim, J., & Fereday, D. (2019). The impact of strong El Niño and La Niña events on the North Atlantic. *Geophysical Research Letters*, *46*, 2874–2883. https://doi.org/10.1029/2018GL081776

Hatzaki, M., Flocas, H. A., Asimakopoulos, D. N., & Maheras, P. (2007). The eastern Mediterranean teleconnection pattern: Identification and definition. *International Journal of Climatology*, *27*(6), 727–737. https://doi.org/10.1002/joc.1429

Higgins, R. W., Leetmaa, A., & Kousky, V. E. (2002). Relationships between climate variability and winter temperature extremes in the United States. *Journal of Climate*, *15*(13), 1555–1572. https://doi.org/10.1175/1520-0442(2002)015<1555:rbcvaw>2.0.co;2

Higgins, R. W., Leetmaa, A., Xue, Y., & Barnston, A. (2000). Dominant factors influencing the seasonal predictability of US precipitation and surface air temperature. *Journal of Climate*, *13*(22), 3994–4017. https://doi.org/10.1175/1520-0442(2000)013<3994:dfitsp>2.0.co;2

Higuchi, K., Huang, J., & Shabbar, A. (1999). A wavelet characterization of the North Atlantic oscillation variation and its relationship to the North Atlantic sea surface temperature. *International Journal of Climatology*, *19*(10), 1119–1129. https://doi.org/10.1002/(sici)1097-0088(199908)19:10<1119::aid-joc414>3.0.co;2-7

Holland, M. M., & Bitz, C. M. (2003). Polar amplification of climate change in coupled models. *Climate Dynamics*, *21*(3–4), 221–232. https://doi.org/10.1007/s00382-003-0332–6

Horel, J. D., & Wallace, J. M. (1981). Planetary-scale atmospheric phenomena associated with the Southern Oscillation. *Monthly Weather Review*, *109*(4), 813–829. https://doi.org/10.1175/1520-0493(1981)109<0813:psapaw>2.0.co;2

Hurrell, J. W. (1995). Decadal trends in the North Atlantic Oscillation: Regional temperatures and precipitation. *Science*, *269*(5224), 676–679. https://doi.org/10.1126/science.269.5224.676

Hurrell, J. W., & Van Loon, H. (1997). Decadal variations in climate associated with the North Atlantic Oscillation. In Climatic change at high elevation sites (301–326, pp. 69–94). Springer. https://doi.org/10.1007/978-94-015-8905-5_4

Jackson, J. E. (2005). A user's guide to principal components (Vol. 587). John Wiley & Sons.

Kanamitsu, M., Ebisuzaki, W., Woollen, J., Yang, S. K., Hnilo, J. J., Fiorino, M., & Potter, G. L. (2002). NCEP-DOE AMIP-II Reanalysis (R-2). *Bulletin of the American Meteorological Society*, *83*(11), 1631–1643. https://doi.org/10.1175/BAMS-83-11-1631

Kapala, A., Mächel, H., & Flohn, H. (1998). Behaviour of the centres of action above the Atlantic since 1881. Part II: Associations with regional climate anomalies. *International Journal of Climatology*, *18*(1), 23–36. https://doi.org/10.1002/(sici)1097-0088(199801)18:1<23::aid-joc226>3.0.co;2-7

Kolstad, E. W., Breiteig, T., & Scaife, A. A. (2010). The association between stratospheric weak polar vortex events and cold air outbreaks in the Northern Hemisphere. *Quarterly Journal of the Royal Meteorological Society*, *136*(649), 886–893. https://doi.org/10.1002/qj.620

Kretschmer, M., Coumou, D., Agel, L., Barlow, M., Tziperman, E., & Cohen, J. (2018). More- persistent weak stratospheric polar vortex states linked to cold extremes. *Bulletin of the American Meteorological Society*, *99*(1), 49–60. https://doi.org/10.1175/BAMS-D-16-0259.1

Kutzbach, J. E. (1967). Empirical eigenvectors of sea-level pressure, surface temperature and precipitation complexes over North America. *Journal of Applied Meteorology and Climatology*, *6*(5), 791–802. https://doi.org/10.1175/1520-0450(1967)006<0791:eeoslp>2.0.co;2

Lamb, P. J., & Peppler, R. A. (1987). North Atlantic Oscillation: Concept and an application. *Bulletin of the American Meteorological Society*, *68*(10), 1218–1225. https://doi.org/10.1175/1520-0477(1987)068<1218:naocaa>2.0.co;2

Leathers, D. J., & Palecki, M. A. (1992). The Pacific/North American teleconnection pattern and United States climate. Part II: Temporal characteristics and index specification. *Journal of Climate*, *5*(7), 707–716. https://doi.org/10.1175/1520-0442(1992)005<0707:tpatpa>2.0.co;2

Leathers, D. J., Yarnal, B., & Palecki, M. A. (1991). The Pacific/North American teleconnection pattern and United States climate. Part I: Regional temperature and precipitation associations. *Journal of Climate*, *4*(5), 517–528. https://doi.org/10.1175/1520-0442(1991)004<0517:tpatpa>2.0.co;2

Li, J., Garshick, E., Huang, S., & Koutrakis, P. (2021). Impacts of El Niño-Southern Oscillation on surface dust levels across the world during 1982–2019. *The Science of the Total Environment*, *769*, 144566. https://doi.org/10.1016/j.scitotenv.2020.144566

Lopez-Bustins, J. A., Martin-Vide, J., & Sanchez-Lorenzo, A. (2008). Iberia winter rainfall trends based upon changes in teleconnection and circulation patterns. *Global and Planetary Change*, *63*(2–3), 171–176. https://doi.org/10.1016/j.gloplacha.2007.09.002
Mallants, D., & Feyen, J. (1990). Defining homogeneous precipitation regions by means of principal components analysis. *Journal of Applied Meteorology and Climatology*, *29*(9), 892–901. https://doi.org/10.1175/1520-0450(1990)029<0892:dhprbm>2.0.co;2
Martinez-Artigas, J., Lemus-Canovas, M., & Lopez-Bustins, J. A. (2021). Precipitation in peninsular Spain: Influence of teleconnection indices and spatial regionalisation. *International Journal of Climatology*, *41*, E1320–E1335. https://doi.org/10.1002/joc.6770
McCabe, G. J., & Dettinger, M. D. (2002). Primary modes and predictability of year-to-year snowpack variations in the western United States from teleconnections with Pacific Ocean climate. *Journal of Hydrometeorology*, *3*(1), 13–25. https://doi.org/10.1175/1525-7541(2002)003<0013:pmapoy>2.0.co;2
Menendez, M., Mendez, F. J., Losada, I. J., & Graham, N. E. (2008). Variability of extreme wave heights in the northeast Pacific Ocean based on buoy measurements. *Geophysical Research Letters*, *35*, 22. https://doi.org/10.1029/2008GL035394
Montgomery, D. C., Peck, E. A., & Vining, G. G. (2012). *Introduction to linear regression analysis* (5th ed.). John Wiley & Sons.
Newman, M., Compo, G. P., & Alexander, M. A. (2003). ENSO-forced variability of the Pacific Decadal Oscillation. *Journal of Climate*, *16*(23), 3853–3857. https://doi.org/10.1175/1520-0442(2003)016<3853:evotpd>2.0.co;2
Ning, L., & Bradley, R. S. (2016). NAO and PNA influences on winter temperature and precipitation over the eastern United States in CMIP5 GCMs. *Climate Dynamics*, *46*(3–4), 1257–1276. https://doi.org/10.1007/s00382-015-2643-9
Notaro, M., Wang, W. C., & Gong, W. (2006). Model and observational analysis of the northeast US regional climate and its relationship to the PNA and NAO patterns during early winter. *Monthly Weather Review*, *134*(11), 3479–3505. https://doi.org/10.1175/MWR3234.1
Park, T. W., Ho, C. H., & Yang, S. (2011). Relationship between the Arctic Oscillation and cold surges over East Asia. *Journal of Climate*, *24*(1), 68–83. https://doi.org/10.1175/2010JCLI3529.1
Philander, S. G. (1990). *El Niño, La Niña, and the southern oscillation* (p. 293). Academic Pres. https://doi.org/10.1175/2010JCLI3529.1
Pinto, J. G., Reyers, M., & Ulbrich, U. (2011). The variable link between PNA and NAO in observations and in multi-century CGCM simulations. *Climate Dynamics*, *36*, 337–354. https://doi.org/10.1007/s00382-010-0770-x
Pithan, F., & Mauritsen, T. (2014). Arctic amplification dominated by temperature feedbacks contemporary climate models. *Nature Geoscience*, *7*(3), 181–184. https://doi.org/10.1038/ngeo2071
Praetorius, S. K. (2018). North Atlantic circulation slows down. *Nature*, *556*(7700), 180–181. https://doi.org/10.1038/d41586-018-04086-4
Rahmstorf, S., Box, J. E., Feulner, G., Mann, M. E., Robinson, A., Rutherford, S., & Schaffernicht, E. J. (2015). Exceptional twentieth-century slowdown in Atlantic Ocean overturning circulation. *Nature Climate Change*, *5*(5), 475–480. https://doi.org/10.1038/NCLIMATE2554
Renwick, J. A., & Wallace, J. M. (1996). Relationships between North Pacific wintertime blocking, El Niño, and the PNA pattern. *Monthly Weather Review*, *124*(9), 2071–2076. https://doi.org/10.1175/1520-0493(1996)124<2071:rbnpwb>2.0.co;2
Richman, M. B. (1986). Rotation of principal components. *Journal of Climatology*, *6*(3), 293–335. https://doi.org/10.1002/joc.3370060305
Richman, M. B., & Lamb, P. J. (1985). Climatic pattern analysis of three-and seven-day summer rainfall in the central United States: Some methodological considerations and a regionalization. *Journal of Applied Meteorology and Climatology*, *24*(12), 1325–1343. https://doi.org/10.1175/1520-0450(1985)024<1325:cpaota>2.0.co;2
Rogers, J., & McHugh, M. (2002). On the separability of the North Atlantic oscillation and Arctic oscillation. *Climate Dynamics*, *19*(7), 599–608. https://doi.org/10.1007/s00382-002-0247-7
Rohli, R. V., Wrona, K. M., & McHugh, M. J. (2005). January northern hemisphere circumpolar vortex variability and its relationship with hemispheric temperature and regional teleconnections. *International Journal of Climatology*, *25*(11), 1421–1436. https://doi.org/10.1002/joc.1204
Ropelewski, C. F., & Jones, P. D. (1987). An extension of the Tahiti-Darwin Southern Oscillation Index. *Monthly Weather Review*, *115*(9), 2161–2165. https://doi.org/10.1175/1520-0493(1987)115<2161:aeotts>2.0.co;2
Savin, N. E., & White, K. J. (1977). The Durbin-Watson test for serial correlation with extreme sample sizes or many regressors. *Econometrica: Journal of the Econometric Society*, *45*(8), 1989–1996. https://doi.org/10.2307/1914122
Shi, J. K., Qian, W., Huang, F., Li, C., & Tang, C. (2021). Characteristics, trend, and precursors of extreme cold events in northwestern North America. *Atmospheric Research*, *249*, 105338. https://doi.org/10.1016/j.atmosres.2020.105338
Sobolowski, S., & Frei, A. (2007). Lagged relationships between North American snow mass and atmospheric teleconnection indices. *International Journal of Climatology*, *27*(2), 221–231. https://doi.org/10.1002/joc.1395
Stidd, C. K. (1967). The use of eigenvectors for climatic estimates. *Journal of Applied Meteorology and Climatology*, *6*(2), 255–264. https://doi.org/10.1175/1520-0450(1967)006<0255:tuoefc>2.0.co;2
Straus, D. M., & Shukla, J. (2002). Does ENSO force the PNA? *Journal of Climate*, *15*(17), 2340–2358. https://doi.org/10.1175/1520-0442(2002)015<2340:deftp>2.0.co;2
Thompson, D. W., & Wallace, J. M. (1998). The Arctic Oscillation signature in the wintertime geopotential height and temperature fields. *Geophysical Research Letters*, *25*(9), 1297–1300. https://doi.org/10.1029/98GL00950
Thompson, D. W., & Wallace, J. M. (2000). Annular modes in the extratropical circulation. Part I: Month-to-month variability. *Journal of Climate*, *13*(5), 1000–1016. https://doi.org/10.1175/1520-0442(2000)013<1000:amitec>2.0.co;2
Tomassini, L., Gerber, E. P., Baldwin, M. P., Bunzel, F., & Giorgetta, M. (2012). The role of stratosphere-troposphere coupling in the occurrence of extreme winter cold spells over northern Europe. *Journal of Advances in Modeling Earth Systems*, *4*(4), M00A03. https://doi.org/10.1029/2012MS000177
Torrence, C., & Compo, G. P. (1998). A practical guide to wavelet analysis. *Bulletin of the American Meteorological Society*, *79*(1), 61–78. https://doi.org/10.1175/1520-0477(1998)079<0061:apgtwa>2.0.co;2
van Loon, H., & Rogers, J. C. (1978). The seesaw in winter temperatures between Greenland and northern Europe. Part I: General description. *Monthly Weather Review*, *106*(3), 296–310. https://doi.org/10.1175/1520-0493(1978)106<0296:tsiwtb>2.0.co;2
Vanhatalo, E., & Kulahci, M. (2016). Impact of autocorrelation on principal components and their use in statistical process control. *Quality and Reliability Engineering International*, *32*(4), 1483–1500. https://doi.org/10.1002/qre.1858
Vavrus, S. J. (2018). The influence of Arctic amplification on mid-latitude weather and climate. *Current Climate Change Reports*, *4*(3), 238–249. https://doi.org/10.1007/s40641-018-0105-2
Walker, G. T., & Bliss, E. W. (1932). World Weather V. *Memoirs of the Royal Meteorological Society*, *4*, 53–84.
Wallace, J. M., & Gutzler, D. S. (1981). Teleconnections in the geopotential height field during the Northern Hemisphere winter. *Monthly Weather Review*, *109*(4), 784–812. https://doi.org/10.1175/1520-0493(1981)109<0784:titghf>2.0.co;2
Wang, C., Chen, S., Song, Z., & Wang, X. (2020). Impacts of the Atlantic warm pool on North American precipitation and global sea surface temperature in a coupled general circulation model. *Climate Dynamics*, *1*, 1163–1181. https://doi.org/10.1007/s00382-020-05527-5

Wang, D., Wang, C., Yang, X., & Lu, J. (2005). Winter Northern Hemisphere surface air temperature variability associated with the Arctic Oscillation and North Atlantic Oscillation. *Geophysical Research Letters*, *32*(16), L16706. https://doi.org/10.1029/2005GL022952

Wanner, H., Brönnimann, S., Casty, C., Gyalistras, D., Luterbacher, J., Schmutz, C., et al. (2001). North Atlantic Oscillation—Concepts and studies. *Surveys in Geophysics*, *22*(4), 321–381. https://doi.org/10.1023/A:1014217317898

Wolter, K., & Timlin, M. S. (2011). El Niño/Southern Oscillation behaviour since 1871 as diagnosed in an extended multivariate ENSO index (MEI. ext). *International Journal of Climatology*, *31*(7), 1074–1087. https://doi.org/10.1002/joc.2336

Wrona, K. M., & Rohli, R. V. (2007). Seasonality of the northern hemisphere circumpolar vortex. *International Journal of Climatology*, *27*(6), 697–713. https://doi.org/10.1002/joc.1430

Zhi, H., Zhang, R.-H., Lin, P. F., Yu, P., Zhou, G. H., & Shi, S. (2020). Interannual salinity variability associated with the central Pacific and eastern Pacific El Niños in the tropical Pacific. *Journal of Geophysical Research: Oceans*, *125*(10), e2020JC016090. https://doi.org/10.1029/2020JC016090